Eur. Phys. J. A **7**, 245–253 (2000)

THE EUROPEAN PHYSICAL JOURNAL A

Emission time scale of light particles in the system Xe+Sn at 50 AMeV. A probe for dynamical emission?

D. Gourio[1], D. Ardouin[2], M. Assenard[2], G. Auger[3], Ch.O. Bacri[4], N. Bellaize[5], A. Benkirane[3], J. Benlliure[3], B. Berthier[6], E. Bisquer[7], B. Borderie[4], R. Bougault[5], P. Box[4], R. Brou[5], J.L. Charvet[6], A. Chbihi[3], J. Colin[5], D. Cussol[5], R. Dayras[6], E. De Filippo[6], A. Demeyer[7], C. Donnet[7], D. Durand[5], P. Ecomard[3], P. Eudes[2], M. Germain[2], D. Guinet[7], L. Lakehal-Ayat[4], P. Lautesse[7], J.L. Laville[3], L. Lebreton[7], C. Le Brun[5], J.F. Lecolley[5], T. Lefort[5], A. Lefèvre[3], R. Legrain[6], N. Le Neindre[5], O. Lopez[5], M. Louvel[5], N. Marie[3], V. Métivier[2], L. Nalpas[6], A. Ouatizerga[4], M. Parlog[8], J. Péter[5], E. Plagnol[4], E. Pollaco[6], A. Rahmani[2], R.Régimbart[5], T. Reposeur[2], M.F. Rivet[4], E. Rosato[9], F. Saint-Laurent[3], S. Salou[3], M. Squalli[4], J.C. Steckmeyer[5], G. Tabacaru[8], B. Tamain[5], L. Tassan-Got[4], E. Vient[5], C. Volant[6], J.P. Wieleczko[3], A. Wieloch[5], K. Yuasa-Nakagawa[5]

[1] GSI mbH, 64291 Darmstadt, Germany
[2] SUBATECH, IN2P3-CNRS et Universitè, 44070 Nantes Cedex, France
[3] GANIL, CEA et IN2P3-CNRS, B.P. 5027, 14076 Caen Cedex, France
[4] IPN, IN2P3-CNRS, 91406 Orsay Cedex, France
[5] LPC, IN2P3-CNRS, ISMRA et Universitè, 14050 Caen Cedex, France
[6] DAPNIA/SPhN, CEA/Saclay, 91191 Gif sur Yvette Cedex, France
[7] IPN, IN2P3-CNRS et Universitè, 69622 Villeurbanne Cedex, France
[8] NIPNE, 76900 Bucharest-Măgurele, Romania
[9] DSFSezione INFN, Université di Napoli "Federico II", 80126 Napoli, Italy

Received: 30 July 1999 / Revised version: 22 November 1999
Communicated by P. Schuck

Abstract. Proton and deuteron correlation functions have been investigated with both impact parameter and emission source selections. The correlations of the system $^{129}Xe + ^{Nat}Sn$ at 50 AMeV have been measured with the 4π INDRA which provides a complete kinematical description of each event. The emission time scale analyzed with a quantum model reveals the time sequence of the light particles emitted by the projectile-like fragment. The short and constant emission time of the proton, independent of the impact parameter, can be attributed to a preequilibrium process.

1 Introduction

The microscopic description of hot nuclear matter is fundamental to the understanding of energetic heavy ion collisions. Many of the theoretical models developed so far suffer from a shortage of observables to directly test the properties of nuclear matter early after the reaction. An example is the time scale of the reaction. By the very nature, experimenters observe only the signals reaching the detectors at infinite time. Subsequently only asymptotic properties of particles leaving the reaction zone are monitored. This shortcoming is partly bypassed in studies using interferometry of light particles [1]- [10]. It has been shown that the two-body correlation function is not only sensitive to emission time and source size, but also to charge and slope parameter of the source [11] which affect the velocity distribution of the particles and thus the relative distance between them.

It is quite obvious that a 4π detector array [12,13] can be superior to a finite angle hodoscope, as used in many previous investigations, provided the granularity (angular resolution), energy threshold, energy resolution and the particle identification are of sufficient quality. A good 4π setup allows minimally biased event selection avoiding many possible distortions.

At GANIL, the system Xe on Sn has been extensively investigated at 50 AMeV using the 4π multidetector INDRA [14–16]. Here experimental data are further analyzed by means of correlation functions aiming at the correlation properties of light particles [17]. They allow to perform event by event the following tasks: (i) determine an 'experimental' impact parameter, (ii) select and characterize the emission sources, and (iii) build the correlation functions. Instead of imposing a spatially fixed particle correlator, we now can use a correlator, which fully

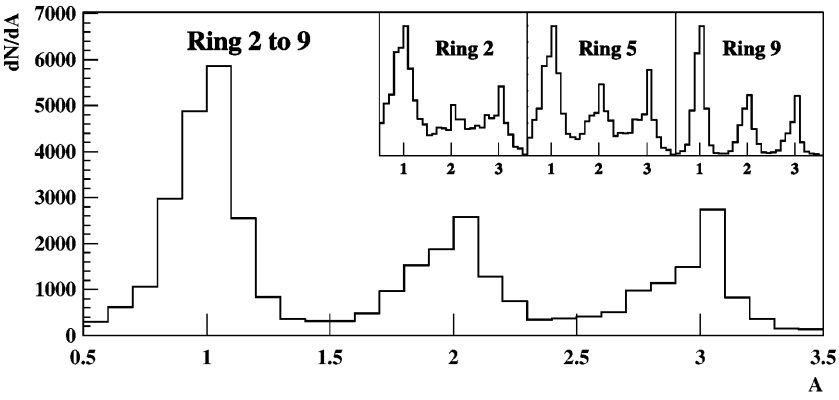

Fig. 1. Light isotopes resolution (Z=1) of the 8 first rings and in the insert for the rings 2, 5 and 9 separately

exploits the event topology. This correlator continuously adapts to the kinematical configuration of every single collision. So each emission process can be characterized individually.

This study focuses on two-proton (p-p), two-deuteron (d-d) and proton-deuteron (p-d) correlation functions for the system $^{129}Xe +^{Nat} Sn$ at 50 AMeV which aims at providing time scales for the emission of the light charged particles. This should shed light on the type of processes, in particular if the reaction is dominated by preequilibrium emission occurring at the early stage of the reaction (typically with times between 0 and 100 fm/c) or by thermal emission from the projectile and target like fragments (typically with times of a few hundreds fm/c). With the knowledge on the chronology pattern, the emission time of deuterons might give a hint to the mechanism for the production of this lowly bound particle in hot nuclear matter. For this purpose the design of the INDRA detector is well-suited [15]. A large range of excitation energies (up to 12 AMeV) is covered and the light charged particle multiplicity which can be measured is adequate for our selection criteria.

With a conventional reaction picture in mind, and supported by recent studies showing that a sizeable fraction of fragments are emitted in the mid-rapidity region [16], only thermalized particles are expected in the forward hemisphere of the momentum space of the projectile-like source. Such an assumption has for example important consequences for the estimation of the excitation energy and the slope parameter of the projectile source [18,19]. Conversely semiclassical calculations of heavy ion reactions in this energy domain have shown that the projectile-like and the prompt emissions from the interacting zone present a large overlap in their rapidity distributions [20]. We have constructed our correlation functions with particles selected in this forward region to find out if the thermalized component is really the single contribution.

The extraction of the emission time was performed with a quantum model whose interesting feature is to take into account the Coulomb effect of the source charge by analytically solving the three-body problem [21,22].

2 INDRA setup and light charged particle resolutions

The experiment was performed at the GANIL facility where the INDRA detector has been installed with a target of 350 $\mu g/cm^2$. The beam intensity was limited to 0.4 nA to avoid a saturation of the data acquisition software.

INDRA [23] has been designed to maximize the detection efficiency of charged particles at intermediate energy. It reaches a total detection efficiency of 90%. The fine granularity chosen is such that double counts stay below 5%. INDRA consists of an array of 336 modules reparted on 17 rings centered along the beam axis. Each module is a telescope composed of an ionization chamber (ChIo) filled with C_3F_8 gas followed by a Cesium Iodide (CsI) scintillator. For forward angles below 45 degrees, the resolution is further improved by insertion of a 300 μm silicon (Si) wafer between the ChIo and the CsI. With $\Delta E - E$ methods in the telescope, the charge identification goes up to Z=54. Isotopic resolution (PID) is obtained for Z=1,2 (and up to Z=5 for ring 2 to 8) by pulse shape analysis of the CsI light output. Lowest energy threshold for the identification of protons and deuterons is 6 MeV using the matrix [CsI(fast) + Si] versus [CsI(slow)].

In particular p-p correlation functions require the resolution of very small relative momenta, less than 20 MeV/c. A minimum relative momentum of 10 MeV/c can be reached for forward angles under 20^o. For the determination of the particle coordinates, the angle from the target to the middle of the detector has been used instead of a random distribution over the spatial extension. The energy resolution of light particles is between 100 keV and 200 keV depending on the module. With exception of INDRA's first ring ($\Delta\Theta = 2^o - 3^o$) which consists of plastic phoswich detectors (NE102 and NE115) for standing higher particle rates in this region, the light isotope separation could be performed on the overall domain.

Figure 1 shows the isotope resolution summed up for rings 2 to 9 ($3^o < \theta < 45^o$). The insert shows it separately for rings 2, 5 and 9. The projectile-like fragments at small angles come out at larger energy. To avoid saturation there, the photomultiplier gains steadily increase from ring 2 to ring 17 by about an overall factor of 10. Subsequently ring 2 has less PID resolution, seen in the

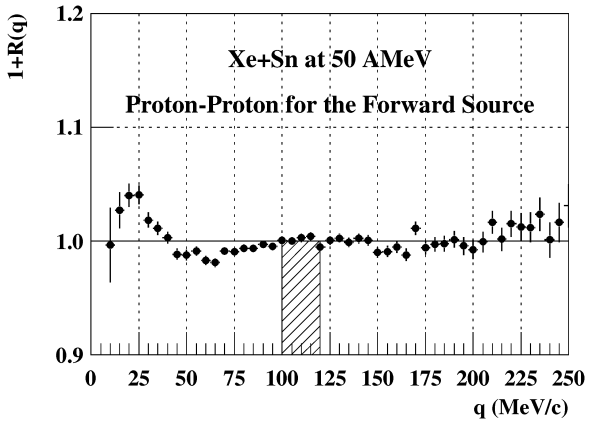

Fig. 2. Two-proton correlation function for the FHPS selection

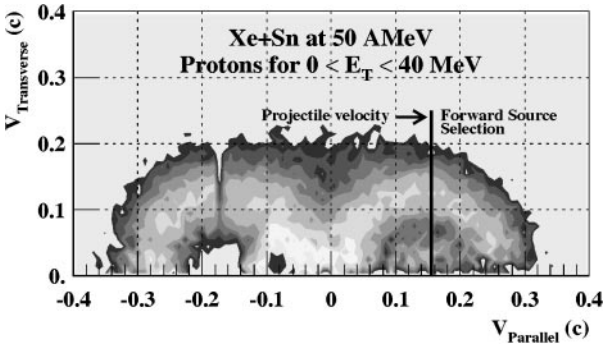

Fig. 3. Invariant velocity plot of the protons in the center of mass for a total light particles transverse energy smaller than 40 MeV which corresponds to a normalized impact parameter larger than 0.9. The average value of the reconstructed forward source is represented by a vertical line at $V_{//} = 0.155c$. This line position is in accordance to the middle of the Coulomb circle. The FHPS is defined by the particles in each event which are faster than the reconstructed forward source velocity

insert to Fig. 1. However the angular resolution of the first rings is superior and therefore they contribute important information to the correlation function at small relative momentum.

The p-p correlation function of Fig. 2 shows the data from the forward hemisphere of the projectile source (FHPS, see Sect. 3) without impact parameter selection. It can be continuously constructed from 10 MeV/c up to 250 MeV/c relative momenta due to the 4π coverage and the good angular resolution (yet the forward source selection slightly increases the minimal relative momentum). The structure in the correlation function at 20 MeV/c is due to the attractive s-wave p-p interaction [1]. There is a Coulomb suppression at very small relative momentum and possibly in the range between 50-75 MeV/c. The normalization has been applied to the data points between 100 and 120 MeV/c which is above any remaining two-body effects and below any kinematical effects at higher momentum. A normalization at lower relative momentum would have introduced a misinterpretation of the correlation effect.

3 Event sorting and source selection

We take in our analysis events in which the total longitudinal momentum of detected ejectiles is above 80% of the initial momentum. We refrain from further cuts, for instance the totally detected charge Z_{tot}, to conserve a representative impact parameter distribution. For most of the events the target like ejectile is lost due to the velocity thresholds. This missing fragment has been kinematically reconstructed and taken into account in the calculation of the momentum tensor and thrust variable. This event class gives an unbiased starting point for the analysis of light particle correlations.

The calculation of the impact parameter is based on the total transverse energy of the light charged particles (Z$\leq$2) whose experimental detection is quite independent of the reaction mechanism. Furthermore a recent analysis of the correlation between the total multiplicity versus the transverse energy (E_T) for that system has demonstrated the validity of E_T [16].

In order to observe impact parameter dependent properties while maintaining sufficient statistics, we have defined three E_T bins for which the correlation function is constructed. The "peripheral", "intermediate" and "central" events have a E_T range between 0-280 MeV, 280-420 MeV and above 420 MeV corresponding to reduced impact parameters in [1-0.65], [0.65-0.35] and smaller than 0.35 respectively.

INDRA allows to build event by event a momentum tensor [24] defined in the center of mass by:

$$Q_{ij} = \sum_{k=1}^{M} \frac{1}{p} p_i(k) p_j(k)$$

where M is the multiplicity of fragments with a charge Z greater than 2, p is the momentum of the k'th particle in M and p_i, p_j two of the Cartesian momentum components. The eigenvectors of this tensor establish a reference frame. The main axis (eigenvector of the largest eigenvalue) gives the average direction of nuclear matter emission. The eigenvectors associated to the two largest eigenvalues define a reaction plane. The FHPS selections and the calculations have been performed with regards to this new reference system. Figure 3 shows the transverse versus the parallel velocity of the protons when E_T is smaller than 40 MeV. Since this selection implies only very peripheral events, a clearer separation of the sources is exhibited.

The next task consists of recognizing the fragments emitted either from the target-like or from the projectile-like source. The thrust variable defined by

$$T = \max_{c_1,c_2} \frac{|\sum_{i\in c_1} \overrightarrow{P_i}| + |\sum_{j\in c_2} \overrightarrow{P_j}|}{\sum_{k=1}^{M} |\overrightarrow{P_k}|}$$

divides up the fragments in two groups c_1 and c_2 corresponding to the two emitting sources. The velocity of each of them is determined by a kinematic reconstruction

within these two ensembles [25]. As an example, the average velocity of the projectile-like source is drawn with a vertical bold line in Fig. 3.

To disentangle the projectile-like source emission from mid-rapidity contributions, we have taken particles with a parallel velocity larger than the projectile source velocity. This region (FHPS) is on the right of the bold line in Fig. 3. In the following, this sample of particles is used as the base for the extraction of the slope parameter in the energy spectra as well as for the construction of the correlation functions. We remind the reader here that our correlator works dynamically within the reference frame, a fact being imperative in order to optimize the FHPS selection.

4 Source parameters: disentangle size and time

4.1 Size

The shape and the height of the correlation function is given by the strength of the interactions which themselves depend on the average distance between the two particles detected in coincidence. This distance depends on the average emission time and on the spatial source extension. The double parametrization can be circumvented only for two extreme cases: at high energy the emission time is set to zero while at low energy the emission time is very long and consequently the source size is negligible [26]. In our energy domain, both parameters are relevant. Using the complete detection by INDRA of all charged products we alternatively can determine the source size directly.

For this estimation, ejectiles are grouped according to $(Z \leq Z_L)$ and $(Z > Z_L)$ where Z_L is an adjusting parameter. In the first group only the particles faster than the projectile-like source velocity are included (particles from the FHPS) and the sum of their charges is multiplied by 2 taking into account the isotropical projectile-like emission. This sum is Z_P in which the additional mid-rapidity contribution mainly composed of light charges is suppressed. The second group contains only the particles faster than the center of mass velocity, the sum of their charges is Z_F. This separate treatment of the heaviest particles (second group) takes into account an asymmetry of emission in the projectile-like reference frame (for example only one big remnant, or two fission fragments). The total charge of the source is $Z_{Total} = Z_P + Z_F$. To test the quality of this procedure, the calculation of Z_{Total} has been performed for different values of the parameter Z_L(2, 4, 8, 10). Figure 4 shows that Z_{Total} only varies by less than 6% with Z_L. For later calculation of Z_{Total} we chose $Z_L = 4$.

For each of the three impact parameter bins we have also defined Z_{Max} as the largest fragment being faster than the center of mass. Z_{Max} decreases with the centrality as expected in the geometrical, simple picture of the collision also shown in Fig. 4. Z_{Total} unexpectedly remains constant.

To estimate the source size, we make two assumptions about the projectile-like source. First, the A_{Total}/Z_{Total} ratio is fixed to the one from the valley of nuclear stability. Secondly, with this value of A_{Total} we determine the source radius r by assuming a normal nuclear density ρ_0 and by simply applying $r = r_0.A_{Total}^{1/3}$ with $r_0 = 1.2$ fm. The central 'single source' events which have a radial flow of 2 AMeV [27] have a very small cross section. This implies that a density different from ρ_0 does not make sense for our calculation even in the central impact parameter bin. The extracted source sizes are given in Table 1. The errors are derivated from the Z_{Total} distribution widths.

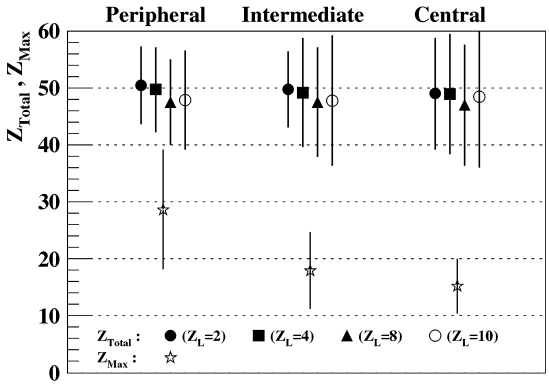

Fig. 4. The reconstructed total charge of the projectile-like Z_{Total} for three centrality bins and for different calculations. The meaning of the parameter Z_L is given in the text. The Z_{Total} dependance on $Z_L$is less than 10% which places confidence in this estimation. The largest fragment Z_{Max} (open stars) gets smaller with centrality as expected in a geometrical picture. This is not the case of Z_{Total} which remains constant

Table 1. Parameters of the projectile-like source. The radius has been calculated from the total reconstructed charge of the source, by assuming a A/Z ratio in the valley of nuclear stability and a normal nuclear density. The slope parameter has been extracted from the energy spectra in the source reference frame

		T_{Proton} (MeV)		$T_{Deuteron}$(MeV)	
Centrality	Radius (fm)	T_1	T_2	T_1	T_2
Peripheral	5.9±0.3	3.7±0.1	9.5±0.1	4.1±0.1	8.9±0.1
Intermediate	5.9±0.4	4.8±0.1	11.3±0.1	6.0±0.1	10.7±0.1
Central	5.9±0.5	5.2±0.1	12.8±0.1	11.3±0.1	*)

*) Only one slope could be extracted

4.2 Slope parameter

We have extracted the *slope parameter* from the experimental energy spectra using the formula for surface emission. As for the source size estimation, we have selected only the protons and the deuterons located in the FHPS region. Their kinetic energy is given in the projectile-like source reference frame. As example for the peripheral collisions, Fig. 5 shows the energy spectra restricted to ring

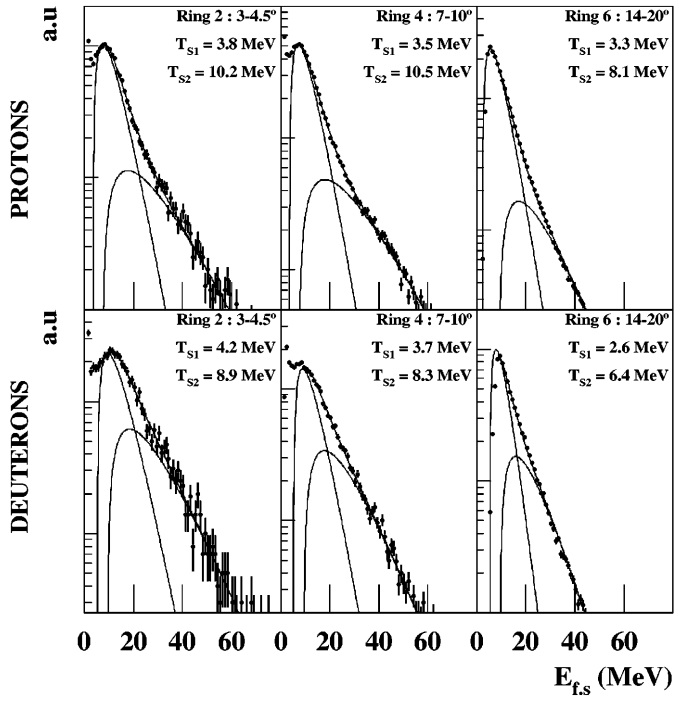

Fig. 5. The energy spectra of the protons (top) and deuterons (bottom) for the ring 2, 4 and 6 in the case of the peripheral collisions. The shapes clearly exhibit two components, better separated in the case of the protons. For comparison reasons the relative scale is the same for all panels

2, 4 and 6 where the double slope is the most clearly visible. The low energy one originates from the projectile-like thermal emission, the other at higher energy, presumably from a preequilibrium emission. We observe that the importance of high energy particles decreases with the radial angle as if this emission were concentrated along the beam axis, and as expected in a Fermi-jet picture [28]. The slope parameters averaged over all the rings included in FHPS are given in Table 1. For the quantum calculation code presented below we have used a weighted average value of the double slopes.

5 Description of the quantum model

The extraction of the emission time has been performed by using the three-body quantum model developed by R. Lednicky [21,22]. This code calculates the quantum statistics for identical particles and the final state interaction by taking into account the nuclear and the Coulomb potentials. The Coulomb repulsion on the particle pair due to the emitting projectile-like source is also included [11]. The three-body problem is analytically solved by making an adiabatic assumption: the relative motion between the two particles has to be much slower than their velocity in the source reference frame. Due to a sizeable angle between neighboring detectors, the small relative momentum region can only be populated by pairs of particles with almost equal velocity. Thus the adiabatic assumption is fulfilled in the region of the signal.

The introduction of the emitter Coulomb effect in the quantum calculation is a new feature brought by this model. We feel that this type of description is required to correctly reproduce the experimental data because the presence of the remnant source charge is intrinsic to the model. In so far it may surpass models where the Coulomb influence of the emitter is only treated as a correction [31]. Limits of this model are certainly related to the static source description [32] which does not take into account the correlation between momentum and position, nor the dynamical emission.

The particle pairs are generated by a static surface emitter describing the projectile-like source with size and slope parameter (see Table 1). The choice of a surface emission instead of a volume one is justified on grounds of the dominance of binary processes [25,30] meaning a big fragment at the speed of the projectile remains in the exit channel. Combined with the fact that no radial flow is observed (see 4.1), the picture of a surface emission of particles seems to be the most appropriate. The time distribution for particle emission follows an exponential decay law with average emission times to be determined from comparison with the data. The energy distribution is taken from the experimental slope parameter. The distributions have been filtered according to the geometrical granularity, including also double counts. In addition, energy and particle identification thresholds as well as the source selection criteria (FHPS) have been folded in.

6 Analysis of the light particle correlation functions

The experimental correlation function is defined by the yield of true coincidences as a function of the two particle relative momentum divided by the so-called false coincidences obtained by the technique of event mixing [33]. It consists of taking two particles from two different events which assures a full decorrelation and has the advantage to use the same sample of events for true and false coincidences. Possible distortions coming from our FHPS selection are then largely eliminated. In general, event mixing introduces an additional term in the relative momentum due to different source velocities. This influence which otherwise would disturb the correlation function is reduced by the impact parameter selection.

6.1 The Proton-Proton correlation function

The p-p correlation functions for the three intervals in impact parameter are represented in Fig. 6. The statistics of 2.3 millions of reconstructed events give a reasonable correlation function above 10 MeV/c relative momentum. In all three event classes, the resonance at 20 MeV/c is clearly visible and well described by a time value of τ=80 fm/c with a surface emission model. A time variation of 25% changes the height of the resonance by a factor of two. This demonstrates the high sensitivity of the correlation function on the emission time parameter. The fact

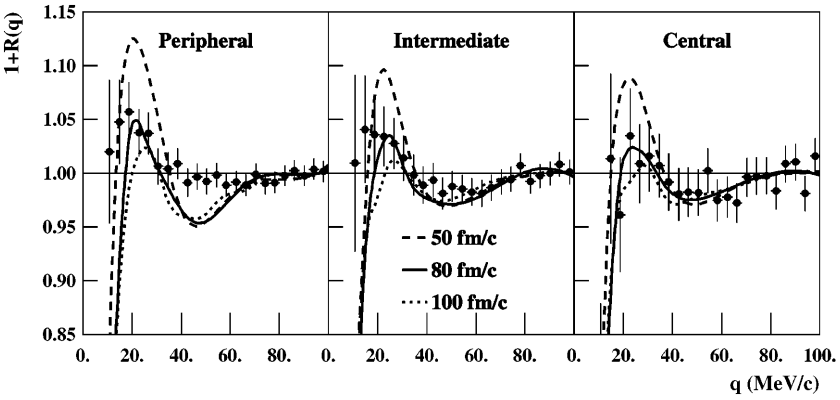

Fig. 6. The experimental p-p correlation functions (black circles) of the projectile-like source for the three impact parameter intervals. Each case has been calculated with different emission times using the source parameters of Table 1. A time of 80 fm/c was found to be the best for all impact parameter bins. The resonance of the calculated function decreases with the centrality because the slope parameter of the emitter increases

that the time estimation strongly depends on the emission description has also been investigated: a simulation using volume break-up, closer to the scenario of a preequilibrium emission, leads to shorter times in the range of 25 fm/c.

The undershoot in the shape of the calculated correlation function visible at 50 MeV/c is induced by the Coulomb repulsion between the two particles. The additional boost due to the repelling charge of the third body (emitting source) shifts the Coulomb suppression, which is usually located at small relative momentum, to higher values. In a pure two body calculation this undershoot almost disappears.

The experimental data also show this behavior at 50 MeV/c for the central events contributing to a very good agreement with the calculation. On the contrary the experimental correlation function for the peripheral events does not show this anticorrelation feature. It is not fully reproduced by the calculation based still on a surface emission. This might indicate the presence of a preequilibrium component, for which no coherent Coulomb influence of a source is expected and for which a volume break-up simulation would be more appropriate. A recent QMD calculation for the system Xe+Sn at 50 AMeV [34] predicts the compression to be maximal at 50 fm/c after the beginning of the collision compatible with the total time of spatial overlap ($\simeq$ 40 fm/c). The end of fragment interaction occurs in this model at 120 fm/c considered as the end of the reaction. Taking this time scale into account, our measured times in between 25 and 80 fm/c are compatible with a preequilibrium emission. It is confirmed by the disappearance of the Coulomb undershoot at 50 MeV/c in the case of the peripheral collisions. The appearance of the double slope in the energy spectra supports this interpretation.

One must ask here, how the emission time alters for a given error in source size. To test this we have reduced the charge from Z=46 to Z=36, simply assuming all the Z=1 particles do not belong to the projectile-like emission. The result for the emission time is then 100 fm/c instead of 80 fm/c which still stays short enough to be compatible with our conclusion saying, these light particles characterize a prompt process of pre-equilibrium emission which covers a large domain of rapidity. By lack of statistics resulting from our source and impact selections, the method of simultaneous determination of the source size and the emission time from parallel and transverse correlation functions [35] could not be tested here.

6.2 The Deuteron-Deuteron correlation function

The d-d correlation function has been constructed on the same base of events as p-p. The normalization has been applied to the data points between 150 and 200 MeV/c. Again the three impact parameter classes have been separately analyzed and the results are shown on Fig. 7. We immediately observe the anticorrelation effect in the d-d correlation function for small relative momenta. Despite the fact that data do not go below 30 MeV/c the fit of the quantum model gives the following results : for peripheral reactions the emission time is as least 200 fm/c, for semi-central reactions it is 100 fm/c and for central it is 25 fm/c. This behavior can be interpreted as an increasing contribution of out-of-equilibrium emission.

Yet the creation of barely bound particles is not the prefered mechanism of hot nuclear matter to dissipate energy. A second scenario could be imagined, assuming the deuteron creation happens only at a certain low density [36]. Then the extracted emission time would give a direct hint on when this state of the nuclear matter is reached during the reaction process. However the double slope of the deuteron energy spectra seems to favor the out-of-equilibrium emission. In the picture of the coalescence model [37], the deuteron formation is directly connected to the proton creation. Consequently it is not surprising to find also two components in the deuteron energy spectra.

In conclusion the process of deuteron production remains an open question. Still we tend to favor the preequilibrium emission over the other explanations. Unfortunately, the present sample of data is insufficient to disentangle more.

6.3 The Proton-Deuteron correlation function and the emission chronology

The correlation function of non-identical particles can give model independent information about their mean order

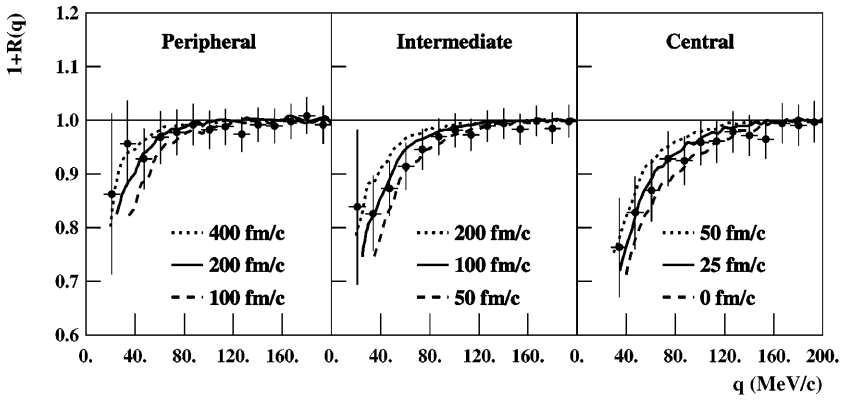

Fig. 7. The experimental d-d correlation functions of the projectile-like source for the three impact parameter bins (black circles). Each case has been calculated with different emission times using the source parameters of Table 1. There is only a weak dependence on the long emission time parameter for the peripheral reactions

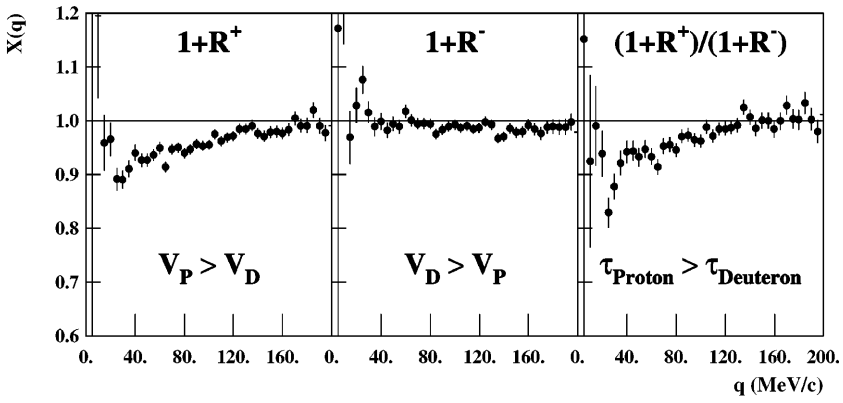

Fig. 8. The experimental proton-deuteron correlation functions of the projectile-like source for the peripheral collisions grouped into two velocity bins (left and middle panel). $1+R^+$ contains all the pairs of particles where the proton was faster than the deuteron. $1+R^-$ is the reverse situation. The ratio of both functions (right panel) which is smaller than unity indicates that the deuteron is on the average emitted earlier than the proton

of emission simply making velocity selections [38–40]. We have applied this method to the p-d correlation function for particles emitted in the FHPS region. The principle is to compare two functions. The first, $(1 + R^+)$, is constructed with pairs where the proton is faster than the deuteron in the projectile-like source reference frame. The second function, $(1+R^-)$, corresponds to the reverse situation. When the first emitted particle is slower than the second, the average distance will be reduced and the Coulomb suppression effect enhanced, and vice versa. The comparison of the two functions gives the mean order of emission as it is shown in Fig. 8 for the peripheral collisions. The Coulomb suppression is more pronounced in $1 + R^+$, which the ratio clearly demonstrates. This means that the deuteron is on average emitted earlier than the proton, namely $\tau_{deuteron} < \tau_{proton}$. The same time sequence is observed for the two other impact parameter selections. It is important to note that this result is only validated between 0-120 MeV/c relative momentum where the anticorrelation effect leaves a measurable signal.

The chronology of emission in p-d spectra of peripheral collision can be considerated as surprising since we just learned from previous paragraphs that the mean emission time is 80 fm/c for p-p and 200 fm/c for d-d. This apparent contradiction can be resolved by postulating that the protons which contribute to p-p are not identical with those contributing to p-d. Indeed the proton energy spectra show a fast and a slow component (Fig. 5). Furthermore, from the energy slopes of Fig. 9, we infer that the

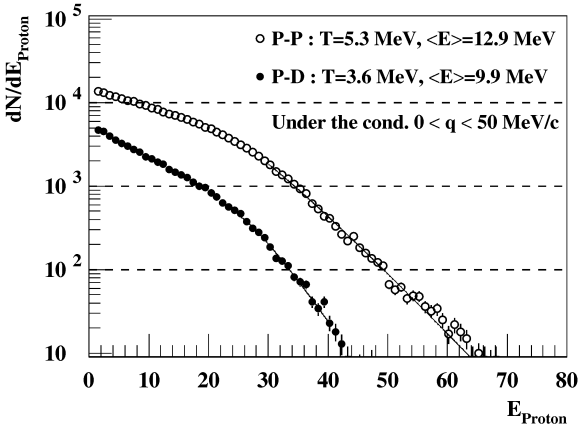

Fig. 9. The kinetic energy of the protons in the projectile-like source frame which contribute to p-p (open circle) or to p-d (black circle) with a relative momentum selection smaller than 50 MeV/c for peripheral collisions. For p-p the average energy and the slope parameter are higher than for p-d

protons of p-p in the relative momentum range of 0-50 MeV/c have a higher mean kinetic energy (12.9 MeV) than the one of p-d in the same range (9.9 MeV). Subsequently it is clear that the p-p correlation function is more influenced by the preequilibrium protons. The extracted times between 25 and 80 fm/c must be seen as an upper limit reflecting the mixing of a fast and a slow component. In the p-d correlation function the situation is different:

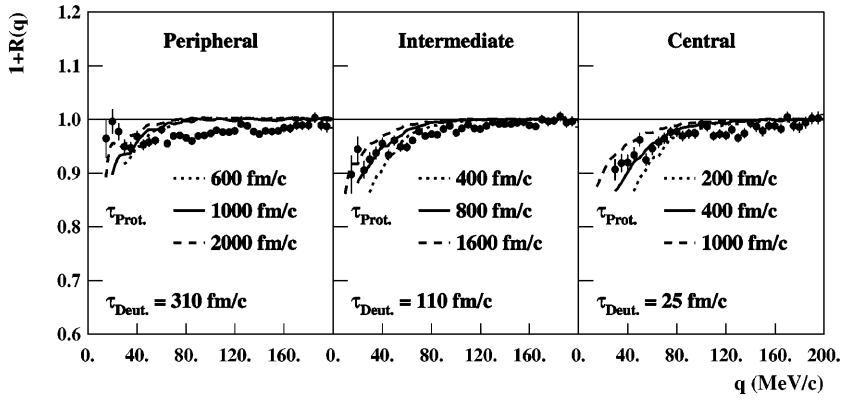

Fig. 10. The experimental proton-deuteron correlation functions of the projectile-like source for the three impact parameter selections (black circles). The calculation (lines) fails to reproduce the data for the peripheral and the intermediate collisions which may reveal the double contribution of fast and slow protons in the interference pattern

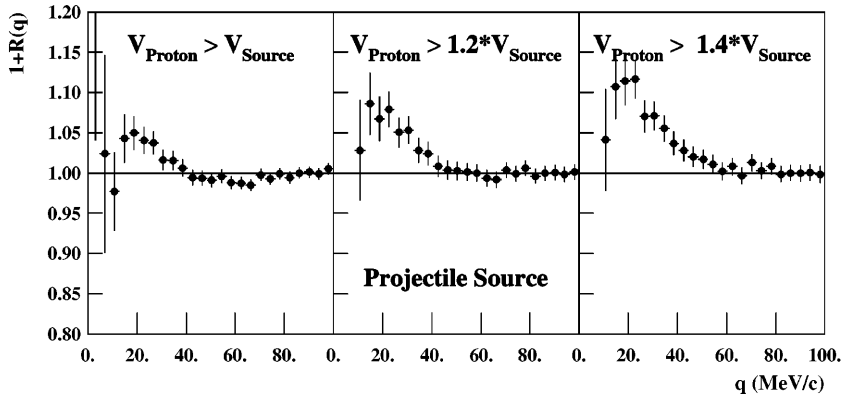

Fig. 11. The experimental proton-proton correlation functions for all impact parameters with increasing selection on their longitudinal velocity in the projectile-like reference frame. The higher resonance indicates a faster emission time

the coincidences of "early" protons with the deuterons are shifted to higher relative momentum value since the speed differs more than for thermal proton-deuteron pairs. Moreover, the functions $1 + R^+$ and $1 + R^-$ are built in the projectile-like source frame. So protons from the interacting zone which feed both correlation functions are per definition faster. Consequently they put only little weight to the emission time order determination. The p-d correlation function informs rather about the thermal protons.

Taking the deuteron emission time extracted from d-d, τ = 310, 110 and 25 fm/c for the peripheral, intermediate and central events respectively, we have deduced the corresponding time for the protons (Fig. 10) and obtained 400 fm/c for central collisions. Unfortunately no satisfying agreement can be found between the quantum model and the p-d data for peripheral and intermediate reactions, possibly due to the different proton contributions, one acting at low the other at high relative momentum. In addition, the description of the source without dynamical features might prevent a better agreement. Therefore the extracted parameters do not retain the meaning of a physical time.

Although both components of protons simultaneously play a role in the correlation function, we can deduce a chronology pattern of the light particle emission. The fast protons from the interacting zone come first, then the deuterons and still later the protons thermally emitted by the projectile-like source. It is possible to better separate the two proton components by making a cut on the parallel velocity as Fig. 11 shows. The clear enhancement of the p-p resonance at 20 MeV/c and the disappearance of the Coulomb suppression at 50 MeV/c reveal the enlarged part of fast protons not feeling the charge of an emitter. The importance of differentiating between short-lived and long-lived emission components and subsequent space-momentum correlations has also been discussed by using source imaging methods [32]. Furthermore, making the plausible hypothesis that fastest particles are emitted earlier than the slowest ones because the available energy is greater at the beginning of the reaction [29], we can extrapolate from the slope parameter pattern an equivalent chronology:

$$T_{Proton\,2} > T_{Deuteron\,2},\ T_{Deuteron\,1} > T_{Proton\,1}$$

7 Conclusion

We have taken the large data set for collisions of Xe on Sn at 50 AMeV which INDRA has accumulated at GANIL to examine correlations of protons and deuterons. Such studies have many attractive aspects in view of the complete detection of all collision residues by a 4π detector. Foremost to name is the unique possibility to well determine the emitting source in particular for symmetric systems

at intermediate energy. In addition each event can be individually characterized in its own frame of reference, due to full charge, angular and energy coverage of INDRA.

The time scale as well as the chronology of emission of light projectile-like particles could be determined from two particles correlation functions interpreted by a full three body quantum code. Total charge measurements as a function of impact parameter indicate possible out-of-equilibrium emission of protons from the forward hemisphere of the projectile source. The observation that the slope parameter of the energy spectra exhibits two components points to a similar conclusion. Strong confirmation of these findings stems from the very short emission time extracted from p-p correlation functions. While this process is expected to dominate in central collisions our study unveils that it also contributes to the forward zone of binary peripheral collisions. We explained in the text how both proton components are not equally shared in p-p and p-d correlation functions. So the whole emission chronology pattern remains self-consistent. It is also in good agreement with the measurement of slope parameters. The short time scale in p-p reveals the presence of fast hot protons from an out-of-equilibrium process. Protons emitted later than the deuterons correspond to the really equilibrated production from the projectile-like source. The light particle emission chronology including the deuteron formation via the $NNN \rightarrow dN$ process has been calculated in the Boltzmann-Uehling-Uhlenbeck (BUU) approach [41]. The theoretical results although for lighter systems are in excellent agreement with the present experimental study.

We would have liked to look into the hydrogenic correlation function in more detail by finer selecting impact parameter intervals. Furthermore, the inclusion of tritons could have given valuable additional information. This task cannot yet be performed on the same footing as with protons and deuterons due to a serious shortage of data statistics.

We therefore suggest to perform a high statistics experiment especially dedicated to light particle correlations. INDRA parameters, optimized toward this goal, could contribute important and still better information on the dynamics of light particle emission.

The authors whish to thank H.Orth for his careful reading of the manuscript, R.Lednicky for discussions and providing his code. D.G acknowledges the support of the ALADIN group at GSI.

References

1. S. Koonin, Phys. Lett. 70B (1977) 43
2. D. Ardouin, Int. Journ. Mod. Phys. E, Vol. 6, N.2 (1997) 3
3. G.J. Kunde et al., Phys. Rev. Lett. 70 (1993) 2545
4. M.A. Lisa et al., Phys. Rev. Lett. 71 (1993) 2863
5. J. Quebert, Ann. de Physique 17 (1992) 99
6. W. Bauer et al., Annu. Rev. Nucl. Part. Sci. 42 (1992) 77
7. W.G. Gong et al., Phys. Rev. C43 (1991) 781
8. D. Boal et al., Rev. Mod. Phys. 62 (1990) 553
9. J. Pochodzalla et al., Phys. Rev. C35 (1987) 1695
10. CORINNE I, Int. Workshop. on Particle Correlations and Interferometry. in Nucl Collisions, Nantes, France (1990). Ed. D. Ardouin (World Scientific) and references therein; CORINNE II, Int. Work.shop on Multiparticle Correlation and Nucl. React. Collisions, Nantes, France (1994). Ed. J. Aichelin, D. Ardouin (World Scientific) and references therein
11. L. Martin et al., Nucl. Phys. A604 (1996) 69
12. R.T. De Souza et al., Nucl. Instr. Meth. A295 (1990) 109
13. A. Gobbi et al., Nucl. Instr. Meth. A324 (1993) 156
14. N. Marie et al., Phys. Rev. C58 (1998) 256-269
15. N. Marie et al., Phys. Lett. B391 (1997) 15
16. J. Lukasik et al., Phys. Rev. C55 (1997) 1906
17. D. Gourio, Thesis of University, Nantes France (1996) unpublished
18. Y.G. Ma et al., Phys. Lett. B390 (1997) 41
19. J. Peter et al., Nucl. Phys. A593 (1995) 95
20. P. Eudes et al., Phys. Rev. C56 (1997) 2003
21. R. Lednicky and V.L. Lyuboshitz, Sov. Jour. Nucl. Phys. 35 (1982) 770
22. R. Lednicky et al., submitted to Nucl. Phys. A
23. J. Pouthas et al., Nucl. Instr. and Meth. A357 (1995) 95
24. J.D Bjorken and S. J. Brodsky, Phys Rev D1 (1970) 1416; S. Brandt et al., Phys. Lett. 35 (1977) 1609
25. V. Metivier et al., XXXIII Int. Wint. Meet. on Nucl. Phys., Bormio, Italy (1995).; V. Metivier et al. subm. to Nucl. Phys. A
26. J. Alexander et al., Phys. Rev. C48 (1993) 2874
27. R. Bougault et al., XXXV Int. Wint. Meet. on Nucl. Phys., Bormio, Italy (1997)
28. H. Fuchs and K. Mohing, Rep. Prog. Phys. 57 (1994) 231 and references therein
29. R. Bougault et al., XXVII Int. Work. on Gross Properties of Nuclei and Nuclear Excitations, Hirschegg, Austria (1999)
30. B. Tamain et al., Heavy-Ion Dynamics and Hot Nuclei. Ed. G. Nebbia and M.N. Namboodiri (World Scientific)
31. Y.M. Sinyukov et al., Physics Letters B432 (1998) 248
32. D. Brown and P. Danielewicz, Phys. Lett. B 398 (1997) 252; D. Brown and P. Danielewicz, Phys. Rev. C57 (1998) 2474
33. D. Drijard et al. Nucl. Instr. and Meth. 225 (1984) 367
34. R. Nebauer and J. Aichelin, Nucl. Phys. A650 (1999) 65; R. Nebauer et al., to be published in Nucl. Phys. A
35. M.A. Lisa et al., Phys. Rev. Lett. 70 (1993) 3709
36. M. Baldo et al., Phys. Rev. C52 (1995) 975
37. S.T. Bulter et al., Phys. Rev. Lett. 7 (1961) 69; A. Schwarzschild et al., Phys. Rev. 129 (1963) 836
38. R. Lednicky et al., Phys. Lett. B 373 (1996) 30
39. C.J. Gelderlos et al., Phys. Rev. C52 (1995) 2834
40. S. Soff et al., Phys. Lett. B449 (1999) 191.; P. Sapienza, Nucl. Phys. A630 (1998) 215
41. W.G. Gong et al., Phys. Rev. C47 (1993) 429